AD-A126 766 MULTI-ZONE MODELING OF IMPURITY REDISTRIBUTION IN ION-IMPLANTED MATERIALS(U) OAK RIDGE ASSOCIATED UNIVERSITIES TENN* R KWOR 15 NOV 82 AFOSR-TR-82-1099 1/1

UNCLASSIFIED AFOSR-82-0161 F/G 20/12 NL

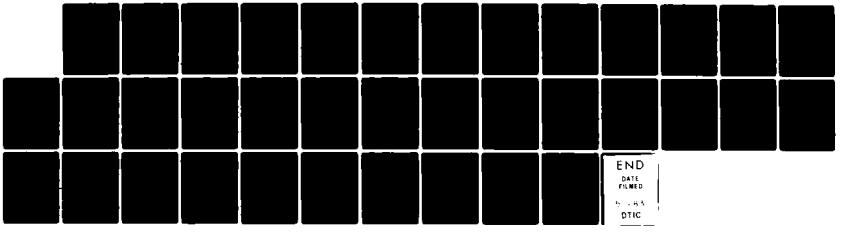

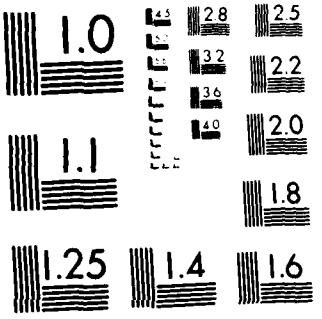

SECURITY CLASSIFICATION OF THIS PAGE (When Data Entered)

REPORT DOCUMENTATION PAGE	READ INSTRUCTIONS BEFORE COMPLETING FORM
1 REPORT NUMBER: AFOSR-TR- 82-1099	2 GOVT ACCESSION NO. AD-A126766
	3 RECIPIENT'S CATALOG NUMBER
4 TITLE (and Subtitle): MULTI-ZONE MODELING OF IMPURITY REDISTRIBUTION IN ION-IMPLANTED MATERIALS	5 TYPE OF REPORT & PERIOD COVERED: FINAL REPORT 4/15/82 - 11/15/82
	6 PERFORMING ORG. REPORT NUMBER
7 AUTHOR(s): RICHARD KWOR	8 CONTRACT OR GRANT NUMBER(s): AFOSR-82-0161
9 PERFORMING ORGANIZATION NAME AND ADDRESS: Department of Electrical Engineering, University of Notre Dame, Notre Dame, IN 46556	10 PROGRAM ELEMENT, PROJECT, TASK AREA & WORK UNIT NUMBERS: 61102F 2306/D9
11 CONTROLLING OFFICE NAME AND ADDRESS: AFOSR/NE, BOLLING AFB DC 20332	12 REPORT DATE: 11/15/82 13 NUMBER OF PAGES: 33
14 MONITORING AGENCY NAME & ADDRESS (if different from Controlling Office)	15 SECURITY CLASS. (of this report): Unclassified 15a DECLASSIFICATION DOWNGRADING SCHEDULE

16 DISTRIBUTION STATEMENT (of this Report)

Approved for public release; distribution unlimited.

17 DISTRIBUTION STATEMENT (of the abstract entered in Block 20, if different from Report)

18 SUPPLEMENTARY NOTES

A paper has been sent to the Electrochemical Society.

19 KEY WORDS (Continue on reverse side if necessary and identify by block number)

ION IMPLANTATION, DIFFUSION, MODELING, SULFUR, MULTI-ZONE, ANNEALING, IMPURITY REDISTRIBUTION

20 ABSTRACT (Continue on reverse side if necessary and identify by block number)

Implanted impurity redistribution has been observed during annealing of many ion-implanted materials. Experimental evidence suggests some position dependence in the redistribution process. The tail region of ion-implanted impurity profiles usually exhibits faster diffusion than the near-surface region. In this paper, a multi-zone model for the redistribution of implanted impurities is presented. The implanted substrate is considered as a stratified medium with zones where a local diffusion equation is obeyed, and an effective diffusion coefficient is

DD FORM 1 JAN 73 1473 EDITION OF 1 NOV 65 IS OBSOLETE

SECURITY CLASSIFICATION OF THIS PAGE (When Data Entered)

20. defined within each zone. The basic formulation of the model and its mathematical background are discussed. The multi-zone equations are solved using the Crank-Nicolson method. A computer program is used to generate a plot of the post-annealing redistributed impurity profile. The model is applied to the case of sulfur-implanted GaAs for dose range of 4×10^{13} to 4×10^{15} cm^{-2}, with energies of 120 keV and 300 keV. Good agreement is obtained between the computer generated profile and the SIMS experimental profile.

Final Report of Research Sponsored by the

AIR FORCE OFFICE OF SCIENTIFIC RESEARCH

MULTI-ZONE MODELING OF IMPURITY REDISTRIBUTION IN ION-IMPLANTED MATERIALS

Prepared by:	Richard Kwor
Academic Rank:	Assistant Professor
Department:	Electrical Engineering
University:	University of Notre Dame
USAF Focal Point Person:	Dr. Y. S. Park
Date:	November 15, 1982
Contract Number:	AFOSR-82-0161

MULTI-ZONE MODELING OF IMPURITY REDISTRIBUTION IN ION-IMPLANTED MATERIALS

by

Richard Kwor

ABSTRACT

Implanted impurity redistribution has been observed during annealing of many ion-implanted materials. Experimental evidence suggests some position dependence in the redistribution process. The tail region of ion-implanted impurity profiles usually exhibits faster diffusion than the near-surface region. In this paper, a multi-zone model for the redistribution of implanted impurities is presented. The implanted substrate is considered as a stratified medium with zones where a local diffusion equation is obeyed, and an effective diffusion coefficient is defined within each zone. The basic formulation of the model and its mathematical background are discussed. The multi-zone equations are solved using the Crank-Nicolson method. A computer program is used to generate a plot of the post-annealing redistributed impurity profile. The model is applied to the case of sulfur-implanted GaAs for dose range of 4×10^{13} to 4×10^{15} cm^{-2}, with energies of 120 keV and 300 keV. Good agreement is obtained between the computer generated profile and the SIMS experimental profile.

ACKNOWLEDGEMENT

The author wishes to thank the Electronics Research Branch of AFWAL Avionics Laboratory, Wright Patternson AFB, Ohio for its valuable support. Special thanks are due to Dr. Y.S. Park whose encouragement and discussion helped the shaping of this research.

The author also wishes to thank Dr. C. Paz de Araujo who has made significant contribution to this research project.

INTRODUCTION

Ion implantation offers a number of advantages in the fabrication of semiconductor devices and is now an established technology for production. Its attractiveness comes from the ability to achieve doping profiles which are controllable, reproducible and sometimes not easily obtained by other techniques. In the designing and characterization of ion implanted devices, it is therefore very important to know or to be able to predict the doping profile. In most cases, the final carrier concentration profile is closely related to the implanted impurity distribution and the post-implantation annealing. High-temperature annealing is necessary for the removal of radiation damages and the activation of implanted atoms. However, the diffusion of the impurity atoms during annealing often results in substantial movement of these atoms, altering the impurity distribution. The pre-annealing impurity distribution is usually described by the profiles of LSS (1), joined half-Gaussian (2), and more recently, the Pearson IV (3, 4). Depending on the implantation conditions, these profiles have various degrees of success. For post-annealing profiles, however, the effect of diffusion must generally be included. The commonly used model for impurity diffusion during annealing assumes an initial Gaussian distribution and a constant diffusion coefficient (5, 6). In the case of capped substrate such as Si_3N_4 on GaAs, the encapsulant is sometimes considered a continuation of the substrate. According to this model, annealing will result in a broader and lower Gaussian distribution. This type of diffusion can only be regarded as an approximation, whereas the actual diffusion of implanted species is, in general, far more complex. Factors such as lattice defects may play an important role in the diffusion mechanics of impurity atoms. During implantation different types of defect occur in

damage clusters around the path of the implanted particle (7). The nature and spatial distribution of radiation damage is extremely complicated. The exact class of defect or defect complex depends on many factors, including the mass and energy of the incident particles and the mass of the target atom. Generally, the damage profile does not coincide with the implanted ion profile; the degree of disparity between these two being a function of the mass difference between the bombarding ion and the lattice atoms. Moreover, when the solid solubility of the implanted species in the substrate is exceeded, as in the case of high dose implantation, precipitates sometimes occur, thus changing the local characteristics of the medium. Clearly, the pre-annealing substrate cannot be considered as a homogeneous medium for diffusion of the implanted impurity atoms. Another important parameter which may also have a considerable influence on the final distribution of implanted ions is the substrate-encapsulant boundary condition. Most encapsulants behave as barriers to outdiffusion, leading to a build up of impurity atoms at the substrate surface, but it is also possible for some to act as sinks. The strain at the substrate-encapsulant interface also has an effect on the diffusion of the implanted impurities (8). This complexity is supported by the experimental evidence that many post-annealing impurity profiles cannot be accurately described by the simple diffusion theory. Examples of long diffusion tails are numerous (9, 10, 11). They suggest that the implanted medium may be characterized by two or possibly more zones with different diffusion constants. This results in a multi-zone modeling scheme for the ion implanted medium. The medium is divided into zones where a local diffusion equation is obeyed with an effective diffusion coefficient which lumps the effects of the defects and possible precipitates. With appropriate boundary and interface conditions, this model can be used to more accurately describe the post-annealing

impurity profiles. In its extended form it can be used to model outdiffusion of implanted species into the encapsulant. In this paper, the basic formulation of the model and its mathematical background are discussed. A computer program is then used to generate a plot of the post-annealing redistributed impurity profile. Reasonable agreement is obtained between the computer generated profile and the SIMS atomic profile of sulfur-implanted Cr-doped GaAs for dose range of 4×10^{13} to 4×10^{15} cm^{-2} with energies of 120 keV and 300 keV. This provides a simple and yet more accurate way of estimating the diffusion coefficients of an ion implanted medium. The advanced matrix formulation of the model allows the computer program to be independent of the initial profile and also virtually independent of constrictions in the boundary conditions. The method is thus very suitable for profile analysis in ion implantation when the initial profiles cannot be defined by analytical forms as in the case of non-Gaussian profiles or multiple implantations.

BASIC FORMULATION OF MULTI-ZONE MODEL

The basic concepts of a double-zone model will first be discussed. In later sections, these basic concepts are generalized for the multi-zone case. Fig. 1 shows the geometry of a double-zone model. The general continuity equation for the position dependent diffusion coefficient is:

$$\frac{\partial C}{\partial t} = \frac{\partial}{\partial x}\left[D(x)\frac{\partial c}{\partial x}\right] \qquad [1]$$

where C(x, t) is the concentration of the implanted impurity atoms, D(x) is the position dependent diffusion coefficient, t is the time and x is the depth. For a double-zone model, each of the two zones is assumed to have a constant diffusion coefficient:

$$D(x) = \begin{cases} D_1 & \text{for } 0 \leq x \leq a^- \\ D_2 & \text{for } a^+ \leq x \leq \ell \end{cases} \qquad [2]$$

where D_1 and D_2 are the effective diffusion coefficients for zone 1 and zone 2 respectively, a is the location of the zone interface and ℓ is the location of the second zone boundary. Thus, Eq. [1] becomes the familiar Fick's second law inside each zone:

$$\frac{\partial C_1}{\partial t} = D_1\frac{\partial^2 C_1}{\partial x^2} \qquad \text{for } 0 < x < a \qquad [3a]$$

$$\frac{\partial C_2}{\partial t} = D_2\frac{\partial^2 C_2}{\partial x^2} \qquad \text{for } a < x < \ell \qquad [3b]$$

where C_1 and C_2 are the concentrations in their respective zones. If the initial condition, i.e. the as-implanted impurity profile is F(x), then

$$C_1(x) = F(x) \qquad \text{for } 0 \leq x < a \qquad [4a]$$

$$C_2(x) = F(x) \qquad \text{for } a \leq x \leq \ell \qquad [4b]$$

The general boundary condition is

$$q_i \frac{\partial C_i}{\partial x} + P_i(x)C_i = f_i(x, t) \qquad [5]$$

at the boundary of the ith zone where the concentration $C_i(x, t)$ is defined. The function $f_i(x, t)$ is seen as a source of impurities located at the boundary. The function $p_i(x)$ is usually a constant related to the absorption or segregation properties of the boundary. If $p_i = 0$, then Eq. [5] reduces to

$$q_i \frac{\partial C_i}{\partial x} = f_i(x, t) \qquad [6]$$

For a reflective boundary, i.e. no diffusing atom crosses it, $\frac{\partial C_i}{\partial x} = 0$, and there is no net flux across the boundary. And if $q_i = 0$ and $p_i \neq 0$, then

$$p_i C_i = f_i(x, t) \qquad [7]$$

An example for this case is $C_i(x, t) = C_B$, the background concentration of impurity in the substrate when ℓ is very large.

In our simple double-zone model, three boundary conditions will be assumed. A perfectly reflective cap is assumed to exist at the surface. Thus,

$$\left.\frac{\partial C_1}{\partial x}\right|_{x = 0} = 0 \qquad [8]$$

For large ℓ, it is reasonable to assume that no diffusing impurity will cross the boundary at $x = \ell$ for the short annealing time used in ion implantation. Then

$$\left.\frac{\partial C_2}{\partial x}\right|_{x = \ell} = 0 \qquad [9]$$

And at the zone interface of x = a, the flux in zone 1 equals that in zone 2. Hence,

$$D_1 \frac{\partial C_1}{\partial x} = D_2 \frac{\partial C_2}{\partial x} \qquad \text{at } x = a \qquad [10]$$

Physically, this means that the interzone boundary is nonabsorbing and does not segregate impurities. Also, in this model, the locations of the zone boundaries are assumed to be time-independent. Then, given an initial condition C(x, 0) = F(x), and with the boundary conditions specified by the Eqs. [8], [9], [10], Eq. [3] can be solved to yield the functions C_1 and C_2 for a specific combination of annealing time and the effective diffusion coefficients in the two zones. The mathematical method is outlined in the next section.

DISCRETIZATION OF THE DIFFUSION EQUATIONS FOR DOUBLE-ZONE MODEL

To solve Eqs. [3a] and [3b] for the double-zone case, the continuous set of space-time points $\{(x, t)\}$ pairs is substituted with a grid of discrete points $\{x_m = m\Delta x \; ; \; t_n = n\Delta t\}$, where Δx and Δt are small intervals of distance and time respectively, m and n are non-negative integers, $m = 0, 1, 2, \ldots, L$; $n = 0, 1, 2, \ldots, T$. At the beginning of first zone, $x_m = 0$, $m = 0$; and at the end of second zone, $x_m = \ell$, $m = L$. The total annealing time is equal to $T\Delta t$. The function $C(x, t)$ at the grid point (m, n) is approximately represented by the point C_m^n. Using the Crank-Nicolson method (12), Eq. [3] can be transformed to:

$$\mathcal{D}_t^+ C_m^n = D_i \mathcal{D}_x^+ \mathcal{D}_x^- \left(\frac{C_m^n + C_m^{n+1}}{2} \right) \qquad [11]$$

where D_i is the diffusion coefficient of the ith zone.

$\mathcal{D}_t^+$ = the finite difference operator for the forward time step.

$$\mathcal{D}_t^+ C_m^n = \frac{C_m^{n+1} - C_m^n}{\Delta t}$$

$\mathcal{D}_x^+$ = the finite difference operator for the forward distance step.

$$\mathcal{D}_x^+ C_m^n = \frac{C_{m+1}^n - C_m^n}{\Delta x}$$

$\mathcal{D}_x^-$ = the finite difference operator for the backward distance step.

$$\mathcal{D}_x^- C_m^n = \frac{C_m^n - C_{m-1}^n}{\Delta x}$$

Eq. [11] can be expanded to a set of equations (13):

$$(1 + \lambda_i) C_m^{n+1} - \frac{\lambda_i}{2} (C_{m+1}^{n+1} + C_{m-1}^{n+1}) = (1 - \lambda_i) C_m^n + \frac{\lambda_i}{2} (C_{m+1}^n + C_{m-1}^n) \qquad [12]$$

where $\lambda_i = \frac{D_i \Delta t}{(\Delta x)^2}$, the normalized diffusion coefficient for the ith zone. The initial condition (n=0) is readily incorporated in this system, and the boundary conditions in the discrete space-grid are:

(1) At the beginning of the first zone, $x_m = 0$, $m = 0$, $i = 1$. Eq. [12] thus becomes

$$(1 + \lambda_1)C_o^{n+1} - \frac{\lambda_1}{2}(C_1^{n+1} + C_{-1}^{n+1}) = (1 - \lambda_1)C_o^n + \frac{\lambda_1}{2}(C_1^n + C_{-1}^n) \qquad [13]$$

If we assume a perfectly reflecting surface, then

$$\left.\frac{\partial C_1}{\partial x}\right|_{x = 0} = 0$$

which in the discretized format becomes

$$\left.\mathcal{D}_x^o C_m^n = \frac{C_{m+1}^n - C_{m-1}^n}{2\Delta x}\right|_{m = 0} = 0$$

where

$$\mathcal{D}_x^o = \frac{\mathcal{D}_x^+ + \mathcal{D}_x^-}{2}$$

therefore

$$\frac{C_1^n - C_{-1}^n}{2\Delta x} = 0 \qquad \text{or} \qquad C_1^n = C_{-1}^n$$

and Eq. [13] becomes

$$(1 + \lambda_1)\, C_o^{n+1} - \lambda_1\, C_1^{n+1} = (1 - \lambda_1)\, C_o^n + \lambda_1\, C_1^n \qquad [14]$$

(2) At the end of the second zone, $x_m = \ell$, $m = L$, $i = 2$,

$\mathcal{D}_x^o C_o^n = 0$, Eq. [12] becomes

$$(1 + \lambda_2)\, C_L^{n+1} - \lambda_2\, C_{L-1}^{n+1} = (1 - \lambda_2)\, C_L^n + \lambda_2\, C_{L-1}^n \qquad [15]$$

(3) At the zone interface, $x_m = a$, $m = A$, and

$$D_1\, \mathcal{D}_x^-\, C_A^n = D_2\, \mathcal{D}_x^+\, C_A^n$$

then the inter-zone equation can be shown to be:

$$\left(1 + \frac{\lambda_1}{2} + \frac{\lambda_2}{2}\right) C_A^{n+1} - \frac{\lambda_1}{2}\, C_{A-1}^{n+1} - \frac{\lambda_2}{2}\, C_{A+1}^{n+1}$$

$$= \left(1 - \frac{\lambda_1}{2} - \frac{\lambda_2}{2}\right) C_A^n + \frac{\lambda_1}{2}\, C_{A-1}^n + \frac{\lambda_2}{2}\, C_{A+1}^n \qquad [16]$$

For $m = 0, 1, 2, \ldots\ldots, L$, the system of equations Eq. [12] can be represented by a matrix equation

$$\underset{\sim}{A}\, \underset{\sim}{C}^{n+1} = \underset{\sim}{B}\, \underset{\sim}{C}^n \qquad [17]$$

where $\underset{\sim}{C}^{n+1} = \begin{bmatrix} C_o^{n+1} \\ C_1^{n+1} \\ \vdots \\ C_L^{n+1} \end{bmatrix}$ and $\underset{\sim}{C}^n = \begin{bmatrix} C_o^n \\ C_1^n \\ \vdots \\ C_L^n \end{bmatrix}$

and $\underset{\sim}{A} =$

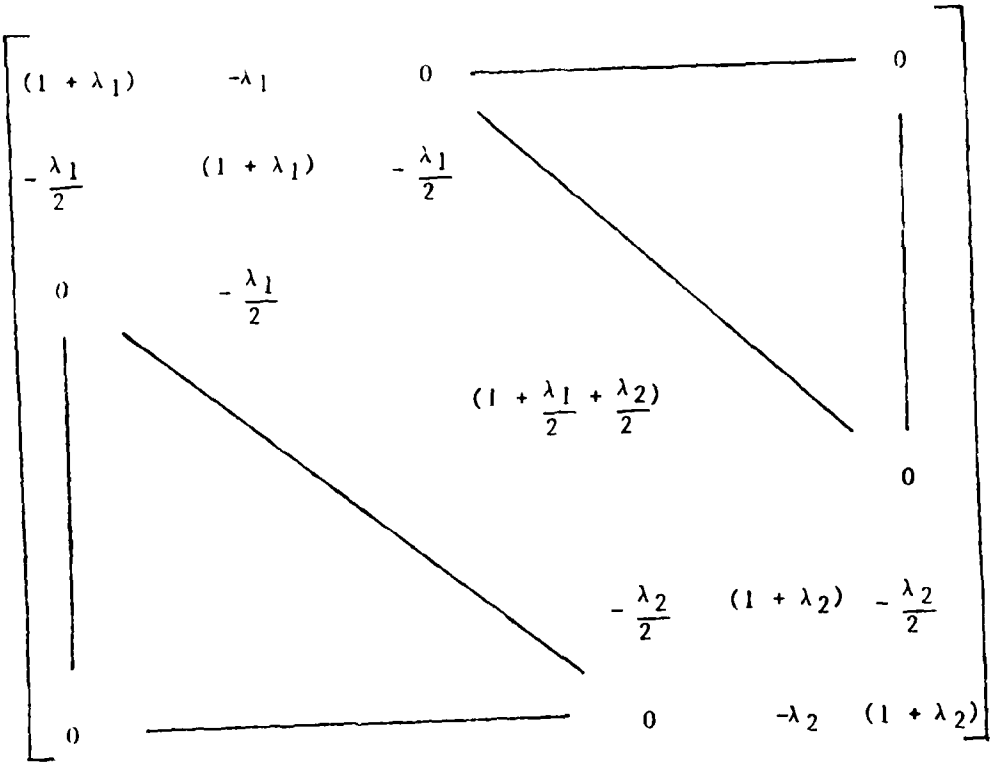

$\underset{\sim}{B} =$

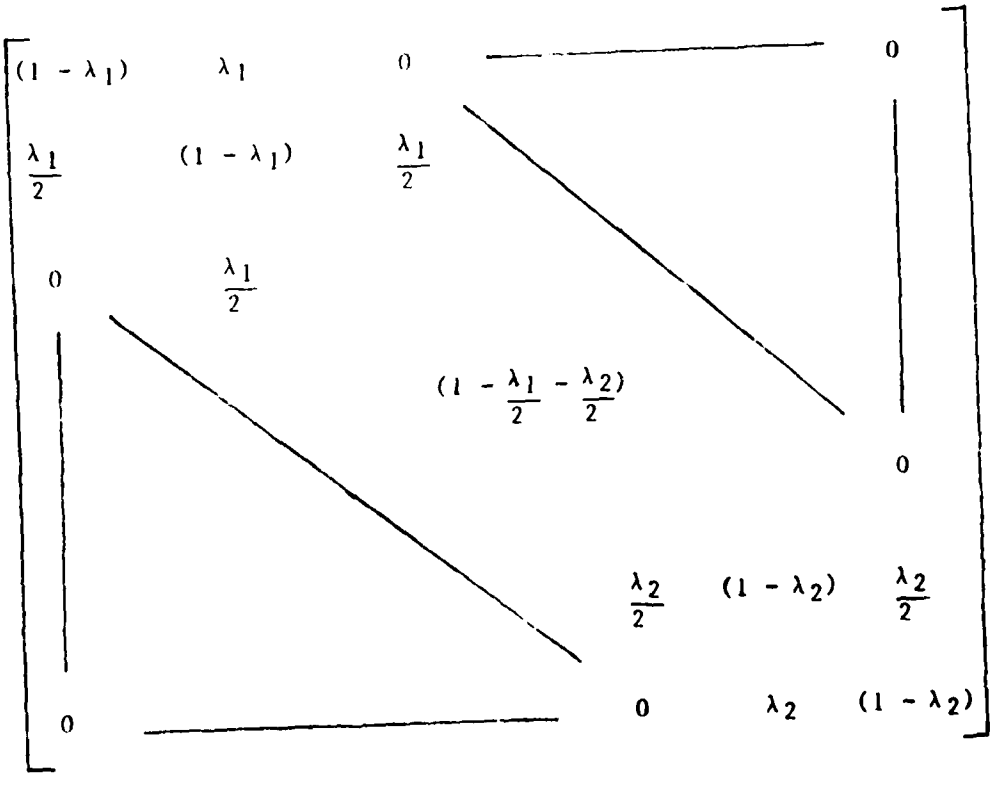

Depending on the surface condition (at $x_m = 0$), the interzone conditions and the last zone boundary condition (at $x_m = \ell$), the $\underset{\sim}{A}$ and $\underset{\sim}{B}$ matrices will take slightly different forms. A computer program is then used to solve the matrix equation Eq. [17] and calculate the values of C_m^n at different grid points (m, n). The redistributed profile after a certain annealing time can then be plotted.

THE MULTI-ZONE MODEL WITH GENERAL BOUNDARY CONDITIONS

The multi-zone model with general boundary conditions (Eq. [5]) follows the same arguments as the double-zone model. Inside the ith zone, where i = 1, 2, 3,.....,I, Fick's law is assumed to be obeyed:

$$\frac{\partial C_i}{\partial t} = D_i \frac{\partial^2 C_i}{\partial x^2} \qquad \text{inside ith zone} \qquad [20]$$

Assume the boundary condition at the surface to be

$$\frac{\partial C_1}{\partial x} + P_1 C_1 = \phi_1(t) \qquad \text{at } x = 0 \qquad [21]$$

And at $x = \ell$ the boundary condition is:

$$\frac{\partial C_I}{\partial t} + P_I C_I = \phi_I(t) \qquad [22]$$

Here $\phi_1(t)$ and $\phi_I(t)$ are time dependent sources (or sinks) at the first and last boundaries. The functions P_1 and P_I are related to the permeability of the boundaries. These boundary conditions are now discretized:

$$D_x^o C_o^s + P_1 C_o^s = \phi_1^s \qquad x_m = 0 \qquad [23]$$

$$D_x^o C_L^s + P_I C_L^s = \phi_I^s \qquad x_m = \ell \qquad [24]$$

where $s = n, n+1$

The first and last equations in Eq. [12] then become:

$$[1 + (1 - \Delta x p_1)\lambda_1]C_o^{n+1} - \lambda_1 C_1^{n+1} + \lambda_1 \Delta x \phi_1^{n+1}$$

$$= [1 - (1 - \Delta x p_1)\lambda_1]C_o^n + \lambda_1 C_1^n - \lambda_1 \Delta x \phi_1^n \qquad [25]$$

$$[1 + (1 + \Delta x p_I)\lambda_I] C_L^{n+1} - \lambda_I C_{L-1}^{n+1} - \lambda_I \Delta x \phi_I^{n+1}$$

$$= [1 - (1 + \Delta x p_I)\lambda_I] C_L^{n} + \lambda_I C_{L-1}^{n} + \lambda_I \Delta x \phi_I^{n} \qquad [26]$$

Eqs. [25] and [26] are seen to reduce to Eqs. [14] and [15] for the double-zone case if $I = 2$, $P_1 = P_I = 0$ and $\phi_1 = \phi_I = 0$ for all $t > 0$. For the multi-zone case, another matrix equation can be obtained:

$$\underset{\sim}{A}\ \underset{\sim}{C}^{n+1} + \underset{\sim}{\phi}^{n+1} = \underset{\sim}{B}\ \underset{\sim}{C}^{n} + \underset{\sim}{\phi}^{n} \qquad [27]$$

where $\underset{\sim}{\phi}^{s} = [\lambda_1 \Delta x \phi_1^{s} \quad 0 \quad 0 \ldots\ldots \lambda_I \Delta x \phi_I^{s}]^T \qquad s = n,\ n+1$

If the inter-zone conditions are kept the same as that for the double-zone case, i.e. assuming no interface resistance or enhancement to particle flow, approaches similar to that for the double-zone model can be used to find the matrices $\underset{\sim}{A}$ and $\underset{\sim}{B}$. And again the redistributed profiles can be calculated given the annealing time and the set of diffusion coefficients for the I zones.

APPLICATION OF THE MODEL TO THE REDISTRIBUTION OF SULFUR IN ION-IMPLANTED GaAs

In this section the multi-zone model described in the previous sections is applied to some profiles of sulfur implanted in <100> oriented Cr-doped semi-insulating GaAs substrate. The implantations were done at room temperature and in a non-channeling direction to doses ranging from 4×10^{13} cm^{-2} to 4×10^{15} cm^{-2}. After implantation, the samples were capped with either Si_3N_4 or SiO_2 and then annealed. There is a significant redistribution of sulfur as a result of diffusion during annealing. As indicated by the SIMS profiles (Figs. 2-5), the as-implanted profile cannot be be adequately described using LSS. Pearson IV distribution was therefore used as the initial condition for the multi-zone model. Using the same approach as that in Ref. (4), the four moments for the Pearson IV distribution were found. These four moments were then fed to the computer which generates the initial condition for the model. Attempts to match the post-annealing profiles for these sulfur implants with Pearson IV distribution have been unsuccessful because of the long diffusion tails involved. However, as will be seen later, the triple-zone model can be used to adequately describe these profiles. Double-zone model has also been tried, but it does not give as good results. As discussed earlier, the model accepts initial condition of any distribution. Pearson IV has been used throughout because it gives satisfactory results for these particular applications. From the SIMS data shown in Figs. 2-5 the different zones in the redistributed profiles are apparent. Depending on the annealing time, temperature, implantation energy and dose, the effective diffusion coefficients in different zones are different. In Figs. 2-4, the impurity concentrations near the surface exceed the solid solubility due to high dose implantation. Precipitation and/or a large amount of unannealed disorder in this region results

in a very small effective diffusion coefficient. Deeper in the substrate, the sulfur atoms diffuse with a larger effective diffusion coefficient. Under such circumstances, significant redistribution of sulfur only occurs in the tail region of the profile. In lower dose implants, there is a much smaller difference in the effective diffusion coefficients of different zones, except in the lower temperature annealing. Fig. 5 gives such an example.

The multi-zone model was applied to four cases. In each case, the Pearson IV moments for the as-implanted profile were found from the SIMS data and used to generate the initial profile. The redistributed profile after annealing was then calculated using a computer. The four cases are discussed below.

The SIMS unannealed and annealed profiles of Cr-doped GaAs implanted with 120 keV, 10^{14} cm^{-2} ^{32}S are shown in Fig. 2. These profiles were reported earlier in Ref. 9. The annealed profile shows a very distinct multi-zone characteristics. Pearson IV distribution was used to describe the as-implanted profile which is seen to deviate substantially from LSS. With the choice of four moments of R_p = 0.1 μm, σ = 0.08 μm, γ = -1.7 and β = 40, a good fit was obtained except near the tail region where the Pearson IV distribution has a slightly shallower penetration. After a 15 minute anneal at 900°C, performed with an Si_3N_4 encapsulant, a pronounced tail appeared in the annealed profile. The tail is seen to start at about 2 x 10^{18} cm^{-3}, which is commonly accepted as the solid solubility of implanted sulfur in GaAs. To model this annealed profile, a triple-zone scheme was used. The Pearson IV distribution with the above mentioned four moments was used as the initial condition. The triple-zone profile with interfaces at 0.2 μm and 0.22 μm, and

three effective diffusion coefficients of $D_1 = 4 \times 10^{-16}$ cm^2/sec, $D_2 = 8 \times 10^{-15}$ cm^2/sec, $D_3 = 1.36 \times 10^{-13}$ cm^2/sec, is shown in Fig. 6.

In Fig. 3, the SIMS unannealed and annealed profiles of Cr-doped GaAs implanted with 120 keV, 10^{15} cm^{-2} ^{32}S are shown. The four moments used in the Pearson IV distribution for the as-implanted profile were $R_p = 0.11$ μm, $\sigma = 0.097$ μm, $\gamma = -2.5$ and $\beta = 40$. Again, a good fit was obtained except near the tail region where the Pearson IV has a shallower penetration, which is common in all the cases reported in this work. After 15 minutes anneal at 900°C, performed with an Si_3N_4 encapsulant, a pronounced tail similar to the above-discussed 10^{14} cm^{-2} dose case appeared. The triple-zone profile for the annealed curve is shown in Fig. 7. The interfaces used were at 0.21 μm and 0.23 μm. The three effective diffusion coefficients were $D_1 = 4 \times 10^{-16}$ cm^2/sec, $D_2 = 8 \times 10^{-15}$ cm^2/sec and $D_3 = 5.6 \times 10^{-13}$ cm^2/sec.

The SIMS data studied in the last case here were also from Ref. 10. Several annealed curves for different temperatures are shown in Fig. 5. Multi-zone characteristics of the profile are more apparent in the lower temperature annealed curves. Triple-zone modeling was performed for the 700°C annealed profile. The SIMS as-implanted profile from Fig. 5 was first calibrated in terms of concentration by integrating the area under the curve and setting it equal to the area under the 700°C annealed curve. The four moments of the Pearson IV were then found: $R_p = 0.24$ μm, $\sigma = 0.12$ μm, $\gamma = -1$ and $\beta = 40$. This initial condition was then used for the triple-zone model. (Fig. 9). The interfaces used were at 0.42 μm and 0.60 μm. The effective diffusion coefficients were $D_1 = 9 \times 10^{-16}$ cm^2/sec, $D_2 = 2.07 \times 10^{-13}$ cm^2/sec and $D_3 = 2.7 \times 10^{-13}$ cm^2/sec.

The above results indicate that for high dose implants, there is very little diffusion in the first two zones, while the effective diffusion

coefficient in the third zone is between 10^{-13} and 10^{-12} cm^2/sec, near the values of sulfur diffusion coefficient reported by other researchers (6, 14, 15, 16). For lower dose and high energy implants, the difference in diffusion coefficients of different zones depends on the annealing temperature. At annealing temperatures below 700°C, there is little diffusion in the first zone, but the diffusion in the third zone is quite fast.

SUMMARY AND DISCUSSION

In all cases studied, reasonable fit was obtained between the triple-zone profile and the corresponding SIMS annealed curve, with best fit obtained in the first and third zones. Since there is a change of as much as several orders of magnitude in the effective diffusion coefficients from the first to the third zones, the second zone is in reality a transition zone in which there is a continuous change of diffusion coefficient. Because of the piece-wise linear nature of the triple-zone model, only one effective diffusion coefficient is chosen for the second zone. Thus the greater the difference between the diffusion coefficients in the first and third zones, the more difficult it is to have an accurate fit of the profile in the second zone. The results from the multi-zone modeling show that the impurity diffusion is related to the implantation energy, dose and annealing temperature. It is believed that at different implantation energy and dose, different damages are created, leading to different effective diffusion coefficients in the third zone. Higher implantation energy results in heavier damage and a larger effective diffusion coefficient in the third zone. Larger doses have a similar effect. On the other hand, the heavy damage near the surface from higher implantation energy or larger dose results in a slow diffusion in that region. Fig. 5 gives a good indication of the influence of annealing temperature on the difference in effective diffusion coefficients of different zones. In this case, when the implantation energy is high and annealing temperature is low (around 700°C), not much of the implantation damages near the surface are removed during annealing, and there is a great difference in the effective diffusion coefficients of the different zones. At higher annealing temperatures, the implantation damages are removed, the difference in diffusion coefficients in different zones is reduced. At 850°C

annealing temperature, the annealed profile has almost lost its multi-zone characteristics.

In summary, the multi-zone model gives a reasonably accurate description of the post-annealing atomic profile for ion-implanted impurities. It also gives some insight of the physical process occuring during the post-implantation annealing, yielding some information of the position dependence of the diffusion. Using the model, effective diffusion coefficients in different zones of the implanted material can be more accurately calculated. This model accepts any profiles as initial condition, and is thus very suitable for profile analysis in ion implantation when the initial profiles cannot be defined by analytical forms as in the case of non-Gaussian profiles.

FIGURE CAPTIONS

Fig. 1. Configuration of a double-zone model for impurity redistribution.

Fig. 2. SIMS unannealed and annealed profiles of Cr-doped GaAs implanted with 120 keV, 10^{14} cm^{-2} ^{32}S. 15 minute anneal was performed with an Si_3N_4 encapsulant.

Fig. 3. SIMS unannealed and annealed profiles of Cr-doped GaAs implanted with 120 keV, 10^{15} cm^{-2} ^{32}S. 15 minute anneal was performed with an Si_3N_4 encapsulant.

Fig. 4. SIMS unannealed and annealed profiles of Cr-doped GaAs implanted with 300 keV, 4×10^{15} cm^{-2} ^{32}S. 20 minute anneal was performed with an SiO_2 encapsulant. (After C. A. Evans et al., Ref. 9).

Fig. 5. SIMS unannealed and annealed profiles of Cr-doped GaAs implanted with 300 keV, 4×10^{13} cm^{-2} ^{32}S. 20 minute anneal was performed with an SiO_2 encapsulant. (After C. A. Evans et al., Ref. 9).

Fig. 6. SIMS profile of 120 keV, 10^{14} cm^{-2} ^{32}S implant annealed at 900°C for 15 minutes; Pearson IV profile initial condition; and triple-zone profile with interfaces at 0.2 μm, 0.22 μm and D_1, D_2, D_3 equal 4×10^{-16}, 8×10^{-15}, 1.36×10^{-13} cm^2/sec respectively.

Fig. 7. SIMS profile of 120 keV, 10^{15} cm^{-2} ^{32}S implant annealed at 900°C for 15 minutes; Pearson IV profile initial condition; and triple-zone profile with interfaces at 0.21 μm, 0.23 μm and D_1, D_2, D_3 equal 4×10^{-16}, 8×10^{-15}, 5.6×10^{-13} cm^2/sec respectively.

Fig. 8. SIMS profile of 300 keV, 4×10^{15} cm^{-2} ^{32}S implant annealed at 840°C for 20 minutes; Pearson IV profile initial condition; and triple-zone profile with interfaces at 0.39 μm, 0.60 μm and D_1, D_2, D_3 equal 9×10^{-15}, 1.44×10^{-13}, 1.98×10^{-12} cm^2/sec respectively.

Fig. 9. SIMS profile of 300 keV, 4×10^{13} cm^{-2} ^{32}S implant annealed at 700°C for 20 minutes; Pearson IV profile initial condition; and triple-zone profile with interfaces at 0.42 μm, 0.60 μm and D_1, D_2, D_3 equal 9×10^{-16}, 2.07×10^{-13}, 2.7×10^{-13} cm^2/sec respectively.

REFERENCES

1. J. Lindhard, M. Scharff and H. E. Schiott, Matt. Fys. Medd. 33, 39(1963).

2. J. F. Gibbons and S. Mylroie, Appl. Phys. Letters, 22, 568 (1973).

3. W. K. Hofker, Phillips Research Reports, Supplement 8, 41(1975).

4. R. G. Wilson, Radiation Effects, 46, 141(1980).

5. T. E. Seidel, A. U. MacRae, Trans. Met. Soc. AIME 245, 491(1969).

6. M. Fujimoto, H. Yamazaki and T. Honda, in "Ion Implantation in Semiconductors," F. Chernow, J. A. Borders and D. K. Brice, Editors, p. 89, Plenum Press, New York (1977).

7. J. F. Gibbons, Proc. IEEE, 60, 1062 (1972).

8. C. P. Lee, R. Zucca, and B. M. Welch, Appl. Phys. Lett. 37, 311 (1980).

9. Y. K. Yeo, Y. S. Park, and R. Kwor, J. Appl. Phys., 53, 1815(1982).

10. C. A. Evans, Jr., C. G. Hopkins, J. C. Norberg, V. R. Deline, R. J. Blattner, R. G. Wilson, D. M. Jamba and Y. S. Park, Paper presented at the Semi-Insulating III-V Materials Conf., Nottingham, England, April 14-16, (1980).

11. L. Vescan, J. Seders, H. Krautle, W. Kutt and H. Beneking, Electron. Lett., 18, No. 12, 533 (1982).

12. A. R. Mitchell and D. F. Griffiths, in "The Finite Difference Method in Partial Differential Equation," John Wiley & Sons, New York (1980).

13. C. Paz de Araujo and R. Kwor, submitted to J. Appl Phys.

14. S. G. Liu, E. C. Douglas, C. P. Wu, C. W. Magee, S. Y. Narayan, S. T. Jolly, F. Kolondra and S. Jain, RCA Review, 41, 227 (1980).

15. H. Matino, Solid-State Electron, 17, 35 (1974).

16. R. G. Frieser, This Journal, 112, No. 7, 697 (1965).

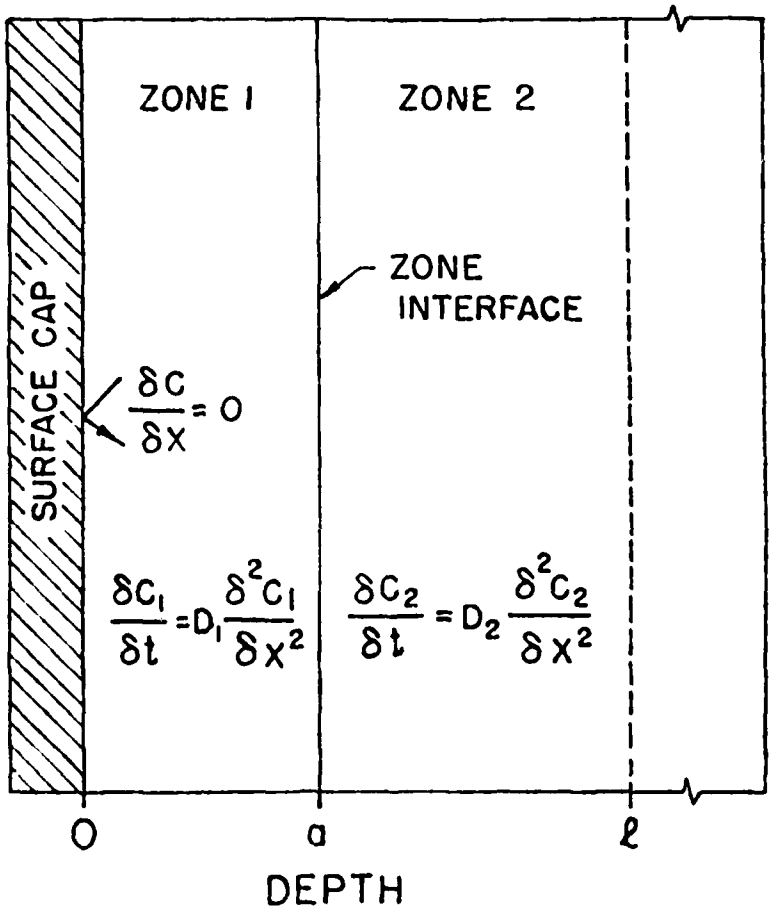
ZONE 1
ZONE 2
ZONE INTERFACE
SURFACE CAP
$\frac{\delta C}{\delta X} = 0$
$\frac{\delta C_1}{\delta t} = D_1 \frac{\delta^2 C_1}{\delta X^2}$
$\frac{\delta C_2}{\delta t} = D_2 \frac{\delta^2 C_2}{\delta X^2}$
0
a
ℓ
DEPTH

Fig. 1

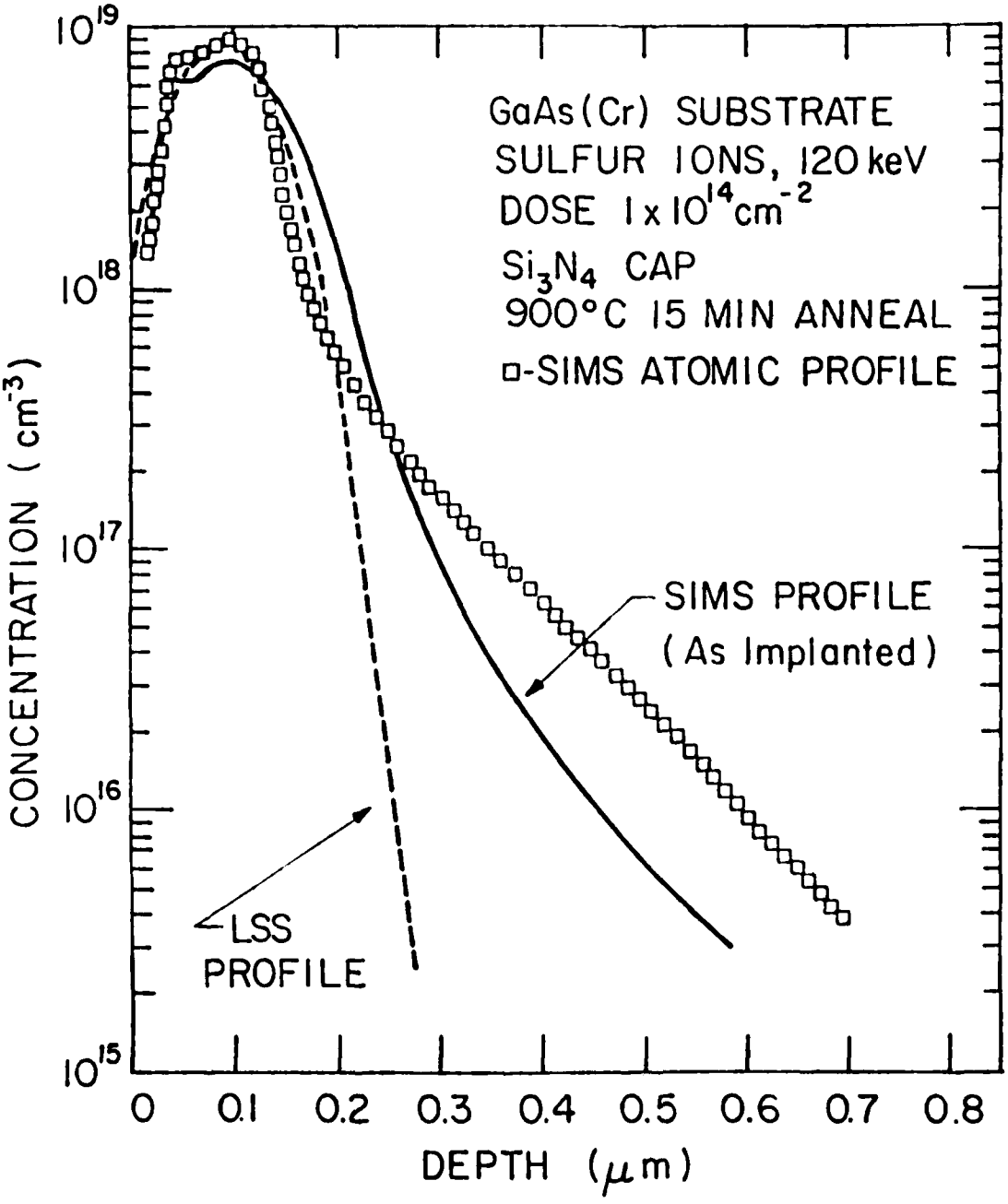
GaAs(Cr) SUBSTRATE
SULFUR IONS, 120 keV
DOSE 1 x 10^14 cm^-2
Si3N4 CAP
900°C 15 MIN ANNEAL
□-SIMS ATOMIC PROFILE
SIMS PROFILE
(As Implanted)
LSS
PROFILE
CONCENTRATION (cm^-3)
DEPTH (μm)
10^19
10^18
10^17
10^16
10^15
0
0.1
0.2
0.3
0.4
0.5
0.6
0.7
0.8

Fig. 2

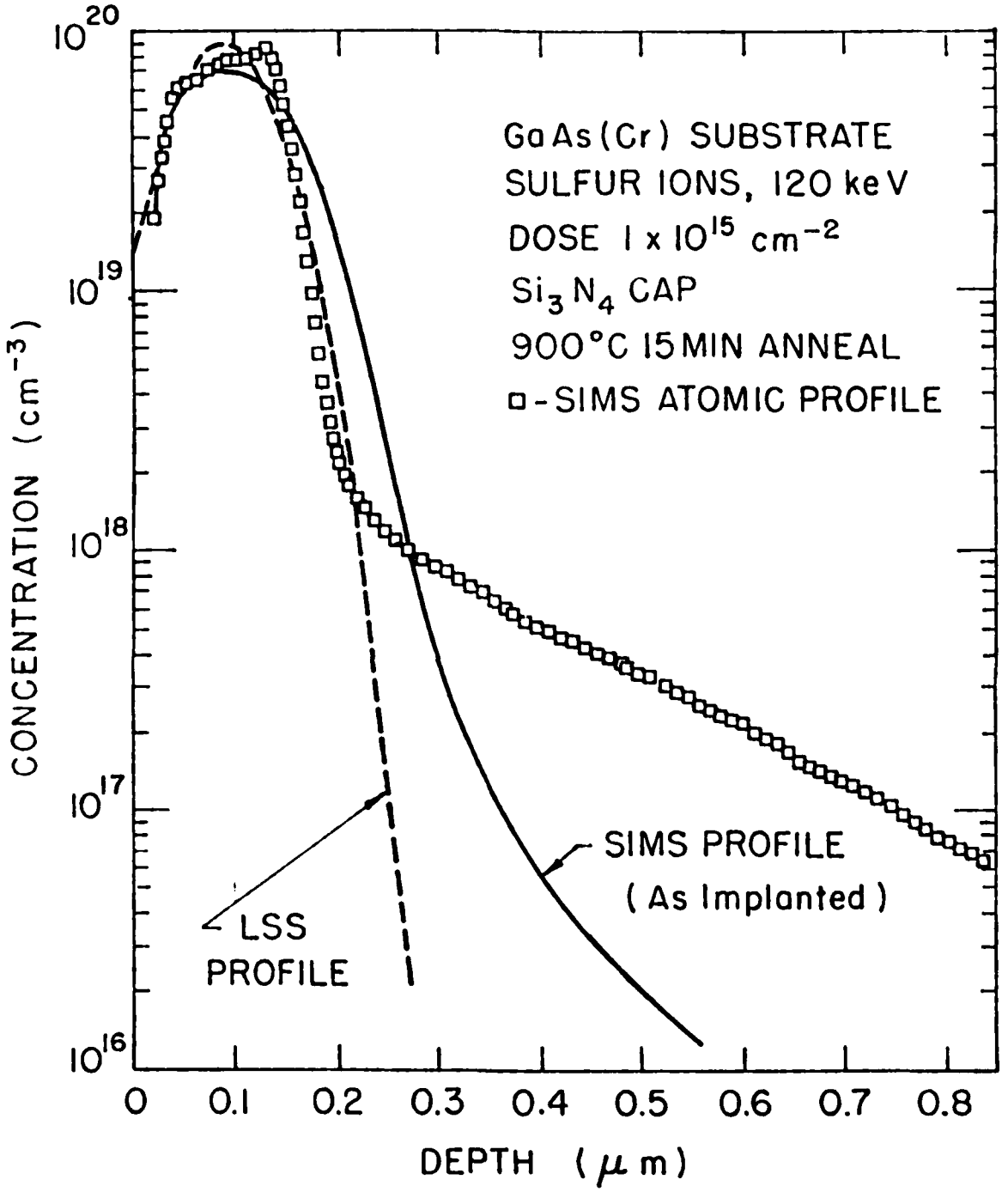
GaAs(Cr) SUBSTRATE
SULFUR IONS, 120 keV
DOSE 1 x 10^15 cm^-2
Si3N4 CAP
900°C 15 MIN ANNEAL
□-SIMS ATOMIC PROFILE
SIMS PROFILE
(As Implanted)
LSS
PROFILE
CONCENTRATION (cm^-3)
DEPTH (μm)
10^20
10^19
10^18
10^17
10^16
0
0.1
0.2
0.3
0.4
0.5
0.6
0.7
0.8

Fig. 3

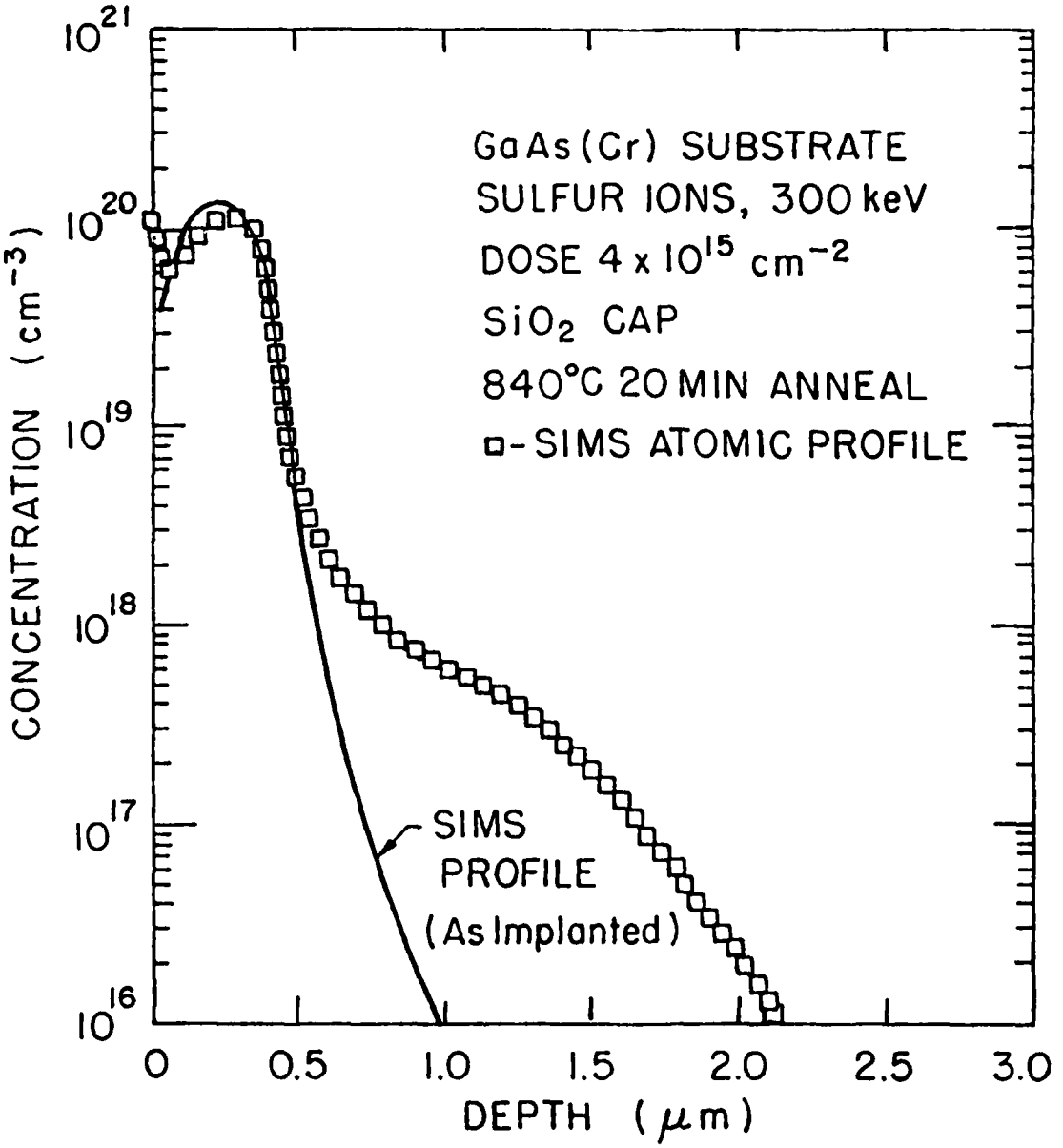
GaAs(Cr) SUBSTRATE
SULFUR IONS, 300 keV
DOSE 4 x 10^15 cm^-2
SiO2 CAP
840°C 20 MIN ANNEAL
□-SIMS ATOMIC PROFILE
SIMS PROFILE (As Implanted)
CONCENTRATION (cm^-3)
DEPTH (μm)
10^21
10^20
10^19
10^18
10^17
10^16
0
0.5
1.0
1.5
2.0
2.5
3.0

Fig. 4

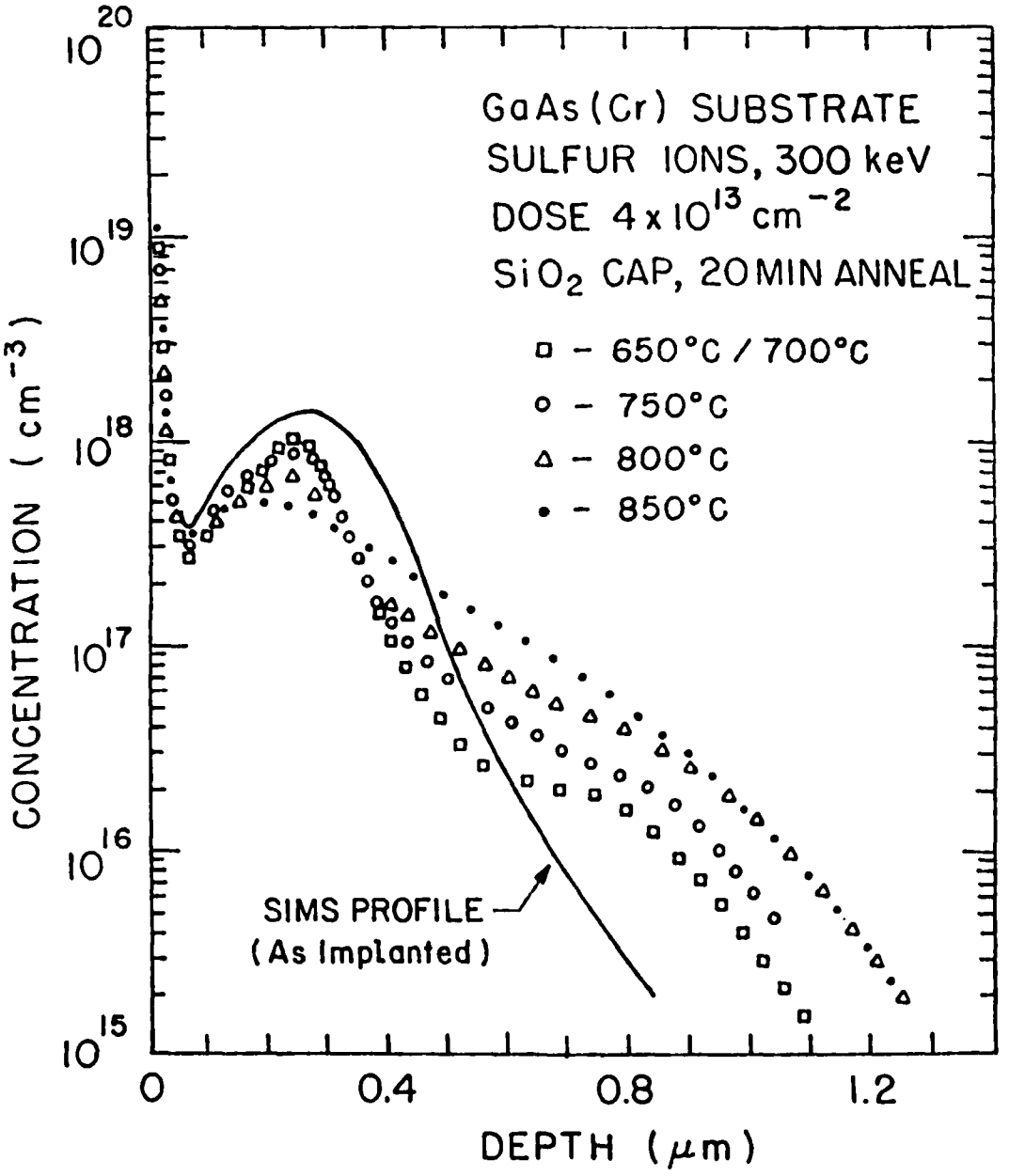
GaAs (Cr) SUBSTRATE
SULFUR IONS, 300 keV
DOSE 4 x 10^13 cm^-2
SiO2 CAP, 20 MIN ANNEAL
□ - 650°C / 700°C
○ - 750°C
△ - 800°C
• - 850°C
SIMS PROFILE
(As Implanted)
CONCENTRATION (cm^-3)
DEPTH (μm)
10^20
10^19
10^18
10^17
10^16
10^15
0
0.4
0.8
1.2

Fig. 5

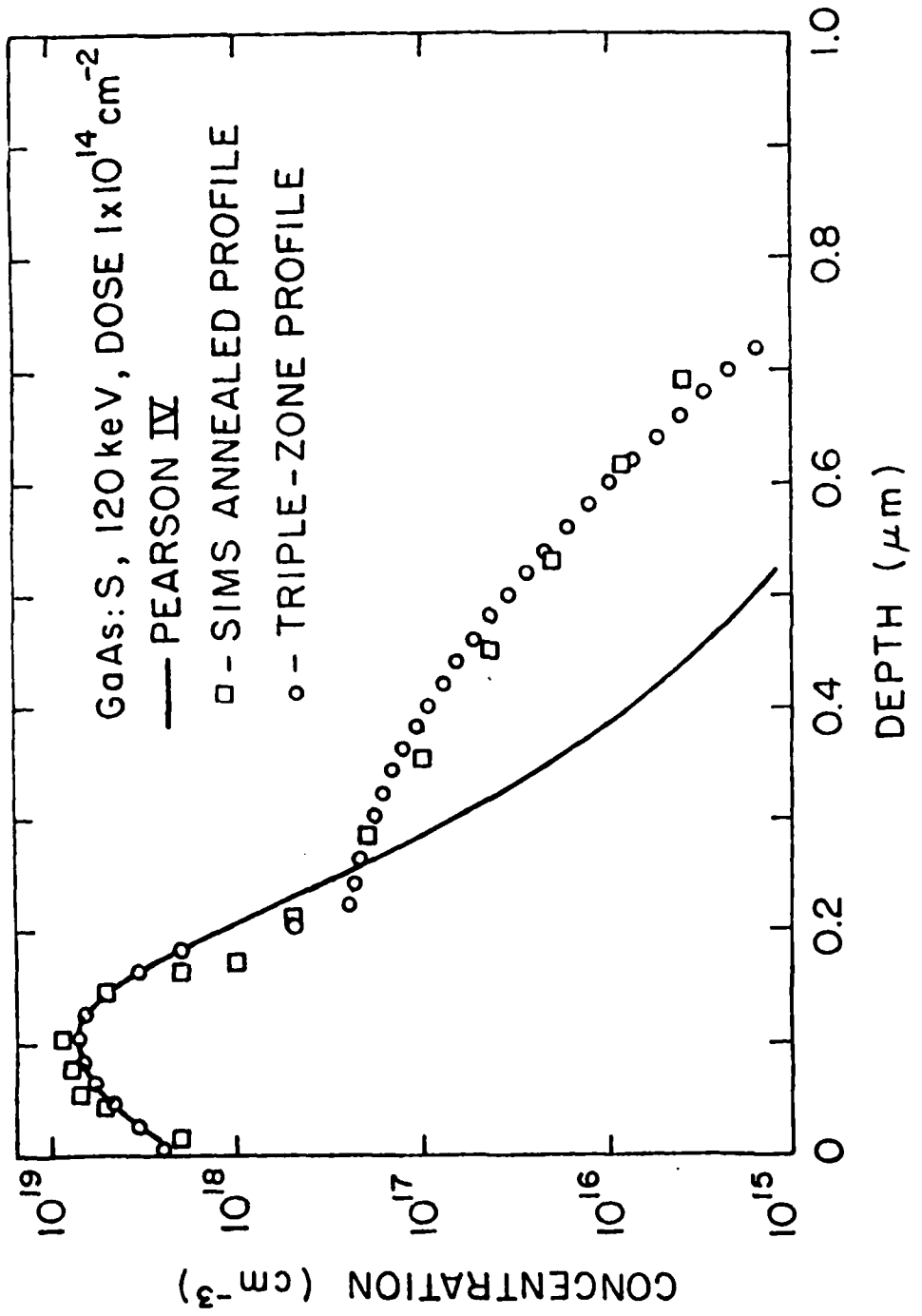
GaAs:S, 120 keV, DOSE 1x10^14 cm^-2
— PEARSON IV
□ - SIMS ANNEALED PROFILE
○ - TRIPLE-ZONE PROFILE
CONCENTRATION (cm^-3)
10^19
10^18
10^17
10^16
10^15
0
0.2
0.4
0.6
0.8
1.0
DEPTH (μm)

Fig. 6

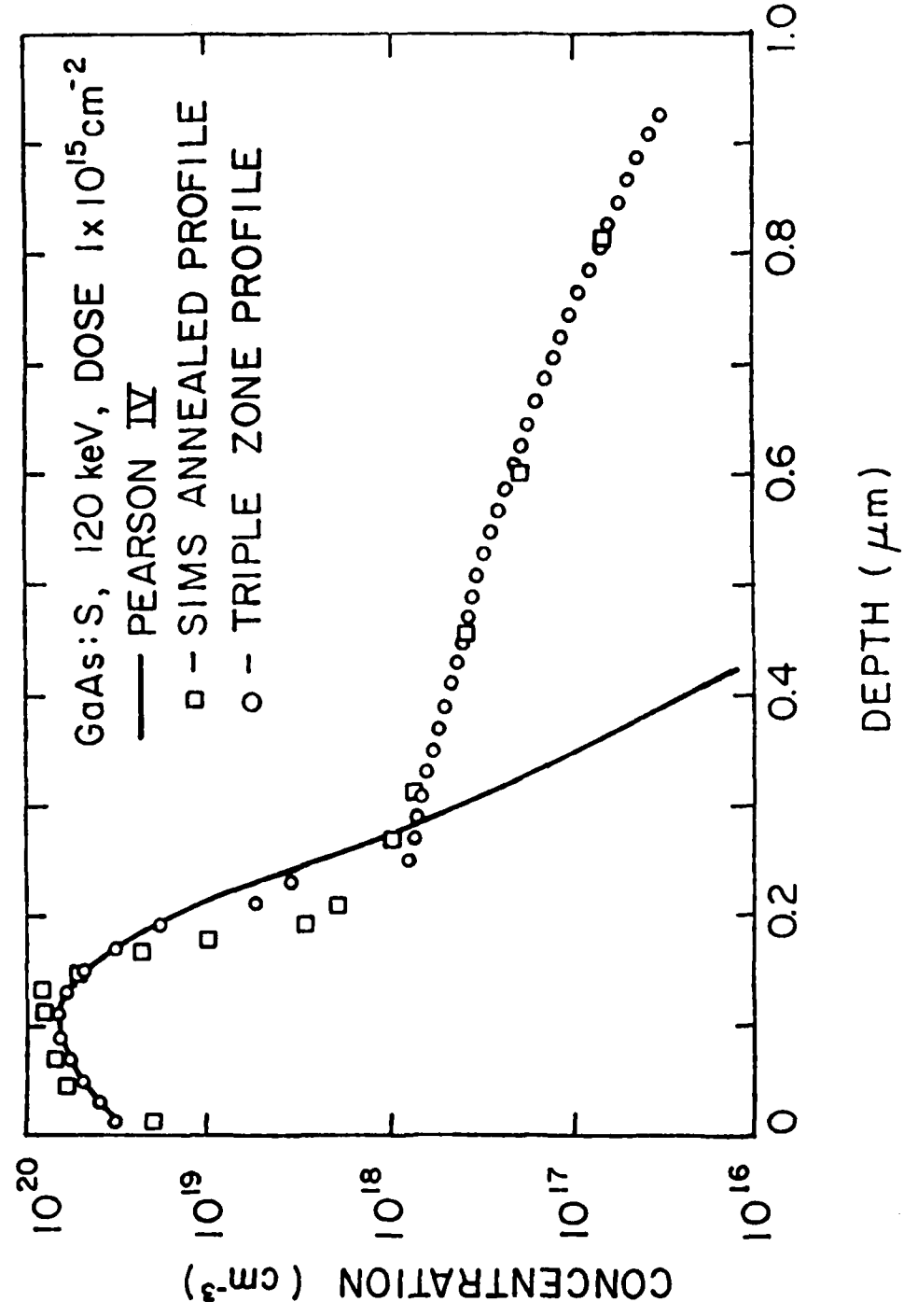
GaAs:S, 120 keV, DOSE 1x10^15 cm^-2
PEARSON IV
□ - SIMS ANNEALED PROFILE
○ - TRIPLE ZONE PROFILE
CONCENTRATION (cm^-3)
10^20
10^19
10^18
10^17
10^16
0
0.2
0.4
0.6
0.8
1.0
DEPTH (μm)

Fig. 7

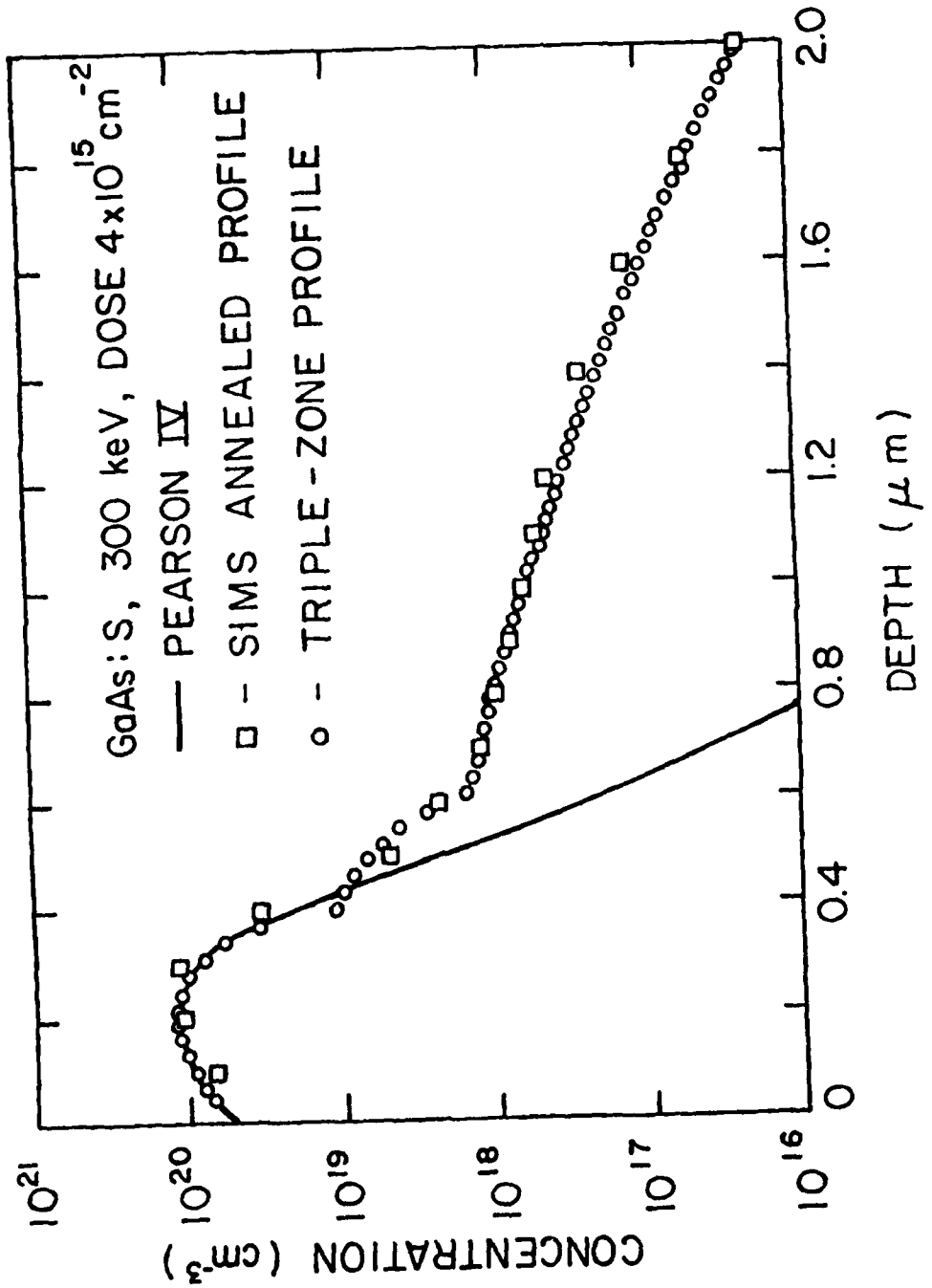
GaAs:S, 300 keV, DOSE 4x10^15 cm^-2
— PEARSON IV
□ - SIMS ANNEALED PROFILE
o - TRIPLE-ZONE PROFILE
CONCENTRATION (cm^-3)
DEPTH (μm)
10^21
10^20
10^19
10^18
10^17
10^16
0
0.4
0.8
1.2
1.6
2.0

Fig. 8

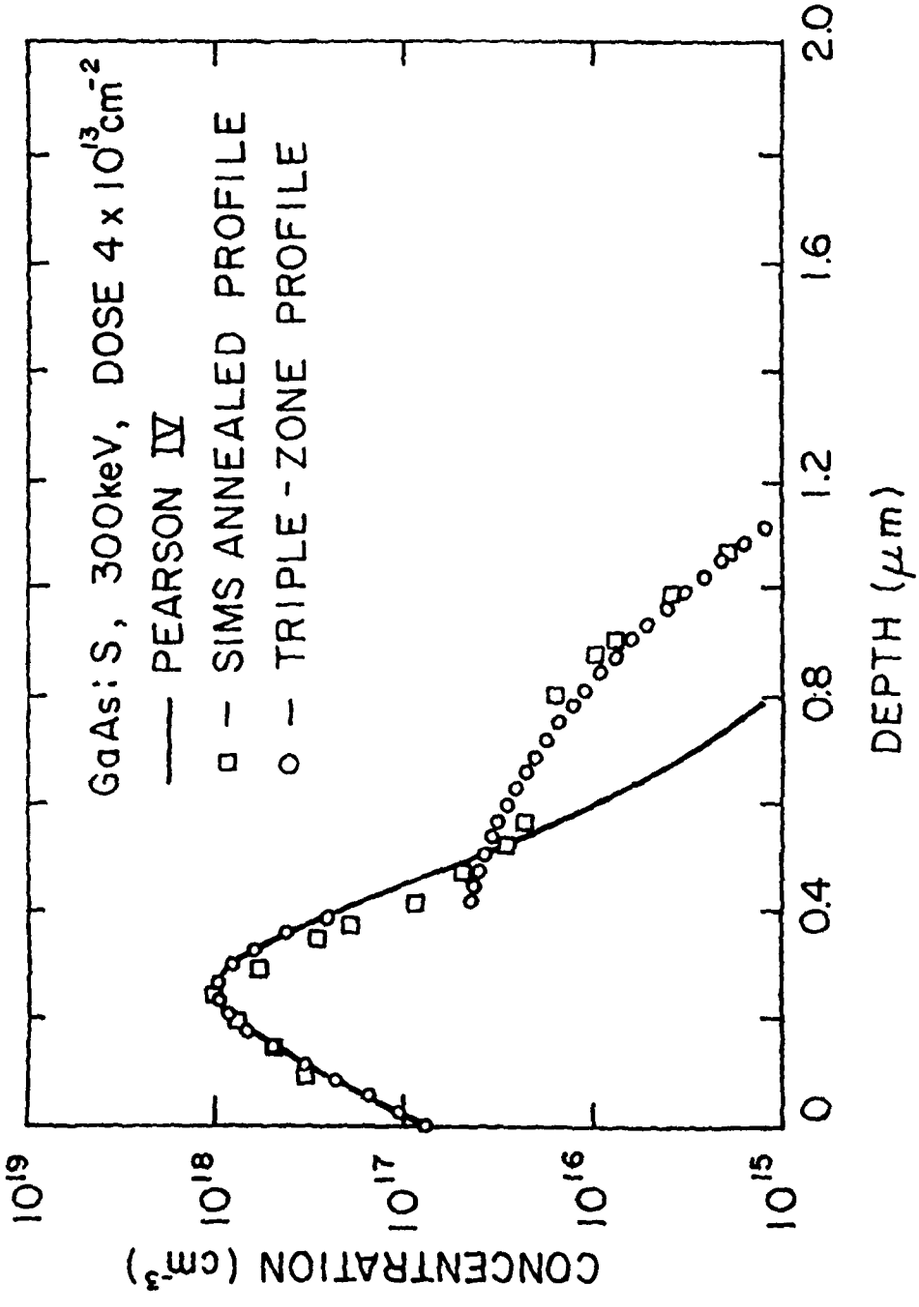
GaAs: S, 300keV, DOSE 4 x 10^13 cm^-2
PEARSON IV
□ — SIMS ANNEALED PROFILE
○ — TRIPLE-ZONE PROFILE
CONCENTRATION (cm^-3)
10^19
10^18
10^17
10^16
10^15
0
0.4
0.8
1.2
1.6
2.0
DEPTH (μm)

Fig. 9


DAT
ILM